TELKOMNIKA Telecommunication Computing Electronics and Control
Vol. 24, No. 6, December 2026, pp. 2037~2047
ISSN: 1693-6930, DOI: 10.12928/TELKOMNIKA.v24i6.28018

Simplifying arterial stiffness estimation: a four-variable machine learning model using dual-site cuff data

Lilia Radjef[1], Tahar Omari[1,2], Karim Baiche[1], Stéphane Carlier[3,4]
[1]Laboratory of Engineering Systems and Telecommunications, Boumerdes University, Boumerdes, Algeria
[2]Faculty of Technology, University of Ain Temouchent, Aïn Témouchent, Algeria
[3]Department of Cardiology, CHU HELORA, Kennedy Site, Mons, Belgium
[4]University of Mons, Mons, Belgium

Article Info

Article history:

Received May 2, 2026
Revised Jul 28, 2026
Accepted Sep 8, 2026

Keywords:

Arterial stiffness
Cardiovascular disease
Machine learning
Pulse transit time
Pulse wave velocity
Random forest

ABSTRACT

Accurate estimation of aortic pulse wave velocity (aPWV) and carotid-femoral PWV (cf-PWV) requires specialised equipment, limiting clinical adoption. This study investigates whether both targets can be estimated from a minimal set of variables obtainable from a standard dual-site cuff measurement: brachial-ankle pulse transit time (ba-PTT), age, systolic blood pressure, and diastolic blood pressure. Using the simulated pulse wave database (PWDB, 1,200 age-stratified subjects), we performed permutation-based feature importance analysis and systematic ablation across eight nested subsets. On this simulated dataset, the optimal four-variable model (set 7, random forest (RF) regression) achieved near-perfect accuracy ($R^2 = 0.9984$, root mean square error (RMSE) = 0.060 m/s for aPWV; $R^2 = 0.9949$, RMSE = 0.113 m/s for cf-PWV); these results should not be interpreted as currently attainable in noisy, real-world clinical settings. Raw ba-PTT outperformed ba-PWV (31% RMSE reduction for aPWV), eliminating the need for anatomical distance measurement; excluding age increased RMSE by 175%. Compared to a previous simulated-data study using radial pressure waveforms (RPW) ($R^2 = 0.98$, RMSE = 0.10 m/s for cf-PWV), the proposed model achieves comparable accuracy with only four scalar features. Its minimal feature set and computational efficiency make it suitable for integration into dual-site cuff devices for ambulatory arterial stiffness monitoring.

This is an open access article under the CC BY-SA license.

Corresponding Author:

Tahar Omari
Faculty of Technology, University of Ain Temouchent
Route de sidi bel abess, N101, Aïn Témouchent 46000, Algeria
Email: tahar.omari@univ-temouchent.edu.dz

1. INTRODUCTION

Arterial stiffness is a major determinant of cardiovascular risk and a key predictor of morbidity and mortality in aging populations, as progressive stiffening raises systolic pressure, increases ventricular afterload, and reduces coronary perfusion [1]. Its independent association with adverse cardiovascular outcomes has been established in large cohorts such as the Framingham Heart Study [2]. Invasive aortic pulse wave velocity (aPWV), obtained via intra-aortic catheterization, remains the gold standard for quantifying aortic wall mechanics [3], reflecting mechanisms such as elastin fragmentation and collagen cross-linking [4]. However, its invasive nature restricts use to specialized interventional settings, which is why carotid-femoral PWV (cf-PWV) has become the accepted non-invasive surrogate, strongly correlated

with aPWV and validated as an independent predictor of cardiovascular events in large epidemiological studies [5]-[7].

Despite this acceptance, cf-PWV measurement remains technically demanding. Acquiring carotid and femoral pulse waves requires trained operators and dedicated tonometry sensors, and the distance travelled by the pulse wave, typically estimated from body-surface landmarks, is a well-known source of bias, since different path-length formulae yield substantially different PWV values [8], [9]. As illustrated in Figure 1 (adapted from Salvi *et al.* [3]), only devices measuring true cf-PWV (complior analyse, PulsePen, SphygmoCor) show strong agreement with invasive aPWV ($r = 0.64 - 0.78$); finger-toe PWV (ftPWV) suffers from path-length bias, while cuff-based devices (BPLab, Mobil-O-Graph) derive stiffness estimates that are almost entirely dependent on age and peripheral systolic pressure rather than on directly measured wave propagation. These constraints make cf-PWV poorly suited to continuous monitoring or integration into portable, patient-operated devices.

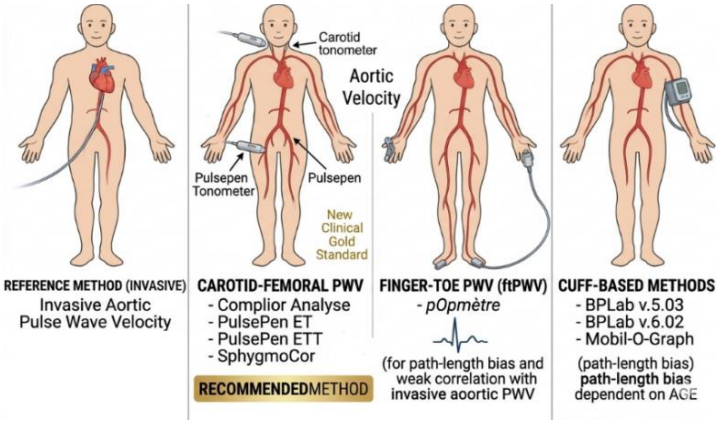


Figure 1. Noninvasive estimation of aortic stiffness: comparison of different approaches. Adapted from Salvi *et al.* [3]; cf-PWV (recommended method), ftPWV, aPWV (invasive gold standard)

Machine learning offers a promising alternative [10], [11]. Jin *et al.* [12] used a recurrent neural network (RNN) on radial pressure waveforms (RPW) to predict cf-PWV ($R^2 = 0.98$ on simulated data), while Chen *et al.* [13] compared several regression models using brachial-ankle (ba-PWV), age, and systolic pressure on a cohort of 1,944 subjects (best $R^2 = 0.81$). Other work has explored convolutional neural network-bidirectional long short-term memory (CNN-BiLSTM) attention architectures for photoplethysmography-based cf-PWV estimation [14] and interpretable models for early aortic-stiffness risk prediction [15], consistent with evidence that arterial stiffening begins as early as childhood in at-risk populations. Martinez-Rodrigo *et al.* [16] reported $R^2 = 0.79$ for aPWV estimation using random forest (RF), gradient boosting, support vector regression (SVR), and neural networks (NN) on 340 clinical subjects. Similarly, interpretable machine learning models have been developed for early prediction of aortic stiffness risk in health examination populations [17], and finger photoplethysmography combined with enhanced pulse wave analysis has shown promise for aortic stiffness estimation [18]. Yet these approaches either rely on specialised waveform signals or on derived PWV indices that themselves require path-length estimation, and none systematically identifies the minimal feature set needed for accurate estimation across both aPWV and cf-PWV references.

This study addresses that gap by testing whether aortic stiffness can be estimated from a minimal, easily obtainable variable set, namely brachial-ankle pulse transit time (ba-PTT), age, systolic blood pressure, and diastolic blood pressure, all derived from a single dual-site cuff measurement without any anatomical distance measurement [19]. We train a RF regression model and systematically evaluate eight feature subsets, ranging from eleven variables down to three, to identify the smallest informative combination and quantify each variable's contribution via permutation-based feature importance. This approach is not intended to replace invasive or cf-PWV measurement, but to offer a practical, fully automated alternative for ambulatory, home-based, or low-resource settings.

The remainder of the paper is organised as: section 2 describes the data source, feature design, RF algorithm, and experimental protocol; section 3 presents and discusses the ablation study results; section 4 concludes the paper.

2. METHODOLOGY

2.1. Overview of the proposed approach

The methodology follows a five-step pipeline:

- Data extraction: a cohort of subjects is extracted from the pulse wave database (PWDB) [20], comprising candidate input variables and two reference standards (aPWV and cf-PWV).
- Feature subset definition: nested feature subsets were defined according to importance ranking, enabling systematic evaluation of the accuracy-complexity trade-off.
- Preprocessing: the dataset is split into training and test sets using stratified sampling. All input features are normalised using Z-score standardisation.
- Model training and hyperparameter optimization: a RF model [21] is trained for each feature subset. Hyperparameters were optimised using five-fold cross-validation.
- Evaluation and subset selection: each model are evaluated on the held-out test set using R^2, root mean square error (RMSE), and pearson correlation r. The optimal subset is selected under a parsimony criterion.

2.2. Data source and preprocessing

We used the open-access PWDB [20], a large-scale simulated database of cardiovascular pulse wave signals. The PWDB contains 4,374 virtual subjects generated by a validated one-dimensional haemodynamic model that incorporates: (i) heart rate and cardiac output, (ii) age-dependent arterial stiffness (via Young's modulus), (iii) peripheral vascular resistance, (iv) vascular geometry (vessel lengths, radii, and wall thicknesses), and (v) measurement sites: aorta, carotid, brachial, radial, femoral, and ankle arteries. The simulation model reproduces realistic pulse wave morphologies and haemodynamic distributions comparable to in vivo measurements [20], consistent with recent work combining imaging modalities such as phase-contrast MRI with machine learning for stiffness prediction [22].

Figure 2 illustrates the arterial segments and corresponding PWV measurements available in the PWDB for a representative 25-year-old subject, including carotid-femoral, carotid-ankle, brachial-femoral, brachial-ankle, radial-ankle, carotid-radial, carotid-brachial, and femoral-ankle segments. From this database, we selected 1,200 subjects aged 25 to 75 years, equally distributed into six age groups (25, 35, 45, 55, 65, and 75 years; 200 subjects per group) to ensure balanced representation across the adult age spectrum, following the stratification protocol adopted in previous PWDB-based arterial stiffness studies.

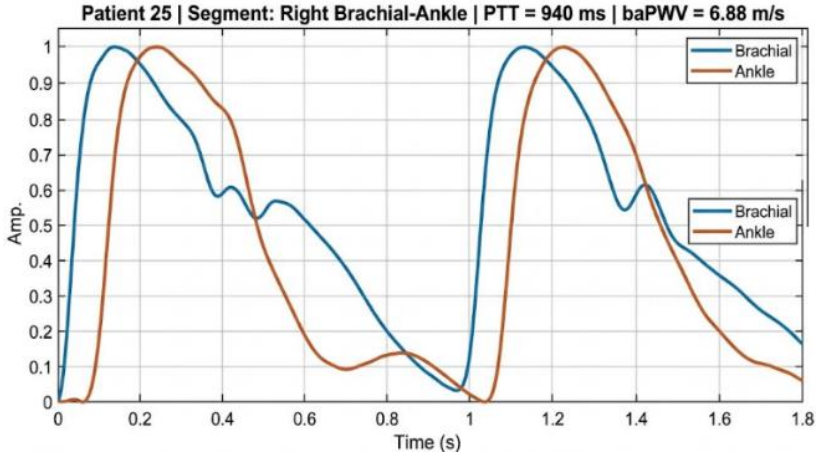


Figure 2. ba-PWV measurements for a representative 25-year-old subject from the PWDB. the PTT (ms) and the corresponding PWV (m/s) are indicated

Table 1 summarises all extracted parameters, including PWV indices, derived indices, haemodynamic parameters, and pulse transit times, stratified by age group. cf-PWV rises progressively with age, from approximately 6.0 m/s at 25 years to 9.9 m/s at 75 years, while the augmentation index (AIx) increases from -0.45% to 36.77% over the same range, reflecting the growing impact of wave reflections on central aortic pressure. Pulse transit times decrease consistently with age, as expected from the inverse relationship between PWV and transit time.

Table 1. Summary of all parameters (mean ± SD) by age group

Parameter	All	25 y	35 y	45 y	55 y	65 y	75 y
PWV (m/s)							
cf-PWV (m/s)	7.82 ± 1.83	6.03 ± 0.65	6.48 ± 0.82	7.38 ± 0.82	8.13 ± 1.09	8.97 ± 1.42	9.90 ± 2.07
aPWV (m/s)	7.32 ± 1.68	5.68 ± 0.51	6.09 ± 0.73	6.90 ± 0.80	7.63 ± 1.06	8.41 ± 1.31	9.24 ± 1.81
ba-PWV (m/s)	8.91 ± 1.84	7.04 ± 0.78	7.50 ± 1.02	8.52 ± 0.92	9.30 ± 1.11	10.15 ± 1.31	10.98 ± 1.79
fa-PWV (m/s)	10.02 ± 1.69	8.43 ± 0.87	8.79 ± 1.10	9.60 ± 0.98	10.32 ± 1.06	11.12 ± 1.20	11.88 ± 1.64
Derived indices							
AIx (%)	17.10 ± 16.47	-0.45 ± 9.12	3.88 ± 9.75	12.55 ± 9.67	20.75 ± 9.87	29.08 ± 10.15	36.77 ± 10.47
Ankle-brachial index (ABI) (ratio)	1.06 ± 0.02	1.08 ± 0.01	1.06 ± 0.01	1.06 ± 0.01	1.05 ± 0.01	1.05 ± 0.02	1.05 ± 0.02
Pulse pressure amplification (PPamp) (mmHg)	1.49 ± 0.23	1.69 ± 0.16	1.68 ± 0.19	1.55 ± 0.17	1.44 ± 0.16	1.33 ± 0.15	1.25 ± 0.14
Haemodynamic parameters (mmHg)							
Systolic blood pressure (SBP) (mmHg)	113.02 ± 11.34	106.19 ± 9.32	109.52 ± 9.82	114.88 ± 9.62	115.98 ± 10.34	115.74 ± 11.26	115.79 ± 13.38
Diastolic blood pressure (DBP) (mmHg)	74.54 ± 6.63	72.06 ± 5.20	75.15 ± 5.67	77.57 ± 5.90	76.65 ± 6.19	74.15 ± 6.77	71.63 ± 7.63
Pulse pressure (PP) (mmHg)	38.48 ± 12.88	34.13 ± 8.30	34.37 ± 9.54	37.31 ± 10.29	39.33 ± 11.99	41.59 ± 13.92	44.15 ± 17.77
Mean blood pressure (MBP) (mmHg)	91.57 ± 6.93	85.92 ± 6.29	89.54 ± 6.45	93.78 ± 6.19	94.31 ± 6.20	93.40 ± 6.30	92.45 ± 6.26
PTT (ms)							
cf-PTT (ms)	7.59 ± 1.86	5.75 ± 0.54	6.21 ± 0.79	7.11 ± 0.86	7.92 ± 1.15	8.82 ± 1.45	9.73 ± 1.98
ba-PTT (ms)	8.12 ± 1.78	6.36 ± 0.50	6.80 ± 0.74	7.65 ± 0.82	8.43 ± 1.10	9.29 ± 1.39	10.17 ± 1.92
fa-PTT (ms)	8.51 ± 1.71	6.84 ± 0.47	7.25 ± 0.70	8.05 ± 0.78	8.80 ± 1.06	9.62 ± 1.35	10.48 ± 1.87

The derived indices AIx, ABI, and PPamp are defined as:

– AIx (%) quantifies the contribution of wave reflections to the central aortic pressure waveform (1):

$$AIx = \frac{P2-P1}{PP} \times 100\% \quad (1)$$

where $P1$ is the pressure at the first systolic peak (incident wave), $P2$ is the pressure at the second systolic peak (reflected wave), and $PP = SBP - DBP$ is the PP.

– ABI ratio assesses peripheral artery patency (2):

$$ABI = \frac{SBP_{ankle}}{SBP_{brachial}} \quad (2)$$

Healthy individuals typically exhibit ABI values between 0.90 and 1.30.

– PPamp dimensionless characterizes the amplification of PP from the central aorta to the peripheral arteries and is defined as (3):

$$PP_{amp} = \frac{PP_{brachial}}{PP_{central}} \quad (3)$$

where, $PP_{\text{brachial}} = SBP_{\text{brachial}} - DBP_{\text{brachial}}$ and $PP_{\text{central}} = SBP_{\text{central}} - DBP_{\text{central}}$. PPamp is a dimensionless haemodynamic index that reflects arterial wave transmission and vascular compliance. In healthy arteries, PP increases as the pressure wave propagates from the aorta to the peripheral arteries due to wave reflection and arterial properties. A lower PPamp indicates reduced PPamp, which is commonly associated with increased arterial stiffness and vascular ageing.

2.3. RF regression

2.3.1. Algorithm description

RF [21] is an ensemble learning method that constructs a multitude of decision trees at training time and outputs the mean prediction of the individual trees for regression tasks. For a dataset $\mathcal{D} = \{(\text{xi}, \text{yi})\}_{i=1}^{N}$ with p-dimensional feature vectors $x_i \in \mathbb{R}^p$ and continuous targets $yi \in \mathbb{R}$, the RF algorithm proceeds:

1) For each tree $b = 1,..,B$:
   a. Draw a bootstrap sample $\mathcal{D}_b^*$ b of size N by sampling with replacement from $\mathcal{D}$.
   b. Grow a regression tree h_b on $\mathcal{D}_b^*$ using the following splitting rule: at each node, randomly select $m = \lfloor\sqrt{p}\rfloor$ candidate features and choose the best split among them (based on mean squared error reduction).
   c. Grow the tree to full depth (or until a minimum leaf size constraint is met) without pruning.
2) The ensemble prediction for a new input x is the average of the individual tree predictions:

$$\hat{y} = \frac{1}{B}\sum_{b=1}^{B} h_b(x) \quad (4)$$

2.3.2. Feature normalisation

All input features were standardised to zero mean and unit variance using the training set statistics:

$$x_{norm} = \frac{(x-\mu_{train})}{\sigma_{train}} \quad (5)$$

where μ_{train} and σ_{train} are computed from the training set. The same normalisation parameters were applied to the test set to prevent data leakage, ensuring that no information from the test set influenced the training or hyperparameter selection process.

2.3.3. Hyperparameter optimisation

Hyperparameters were optimised using a grid search combined with five-fold cross-validation (CV) on the training set. Table 2 presents the search space explored.

Table 2. Hyperparameter search space

Hyperparameter	Symbol	Values explored
Number of trees	B	{100, 300, 500}
Minimum leaf size	min_leaf	{1, 2, 5}
Features per split	m	⌊√p⌋ (automatic)

For each combination (B, min_leaf), we performed five-fold CV:

a. Partition the training set into five disjoint folds.
b. For each fold $k = 1,\ldots,5$:
   – Train a RF on the remaining four folds.
   – Evaluate on fold k using RMSE.
c. Compute the average RMSE across the five folds $RMSE_{CV} = \frac{1}{5}\sum_{k=1}^{5} RMSE_k$.

The optimal hyperparameters (B^*, min_leaf^*) were selected as those minimising $RMSE_{CV}$.

2.3.4. Final model training

After hyperparameter selection, a final RF model was trained on the entire training set (960 subjects) using the optimal hyperparameters. This model was then evaluated on the held-out test set (240 subjects).

2.4. Performance metrics

The following metrics were computed on the test set to evaluate model performance:

2.4.1. Coefficient of determination (R^2)

$\overline{y}_{train}$ is the mean of the target variable in the training set. R^2 represents the proportion of variance in the target explained by the model.

$$R^2 = 1 - \frac{\sum_{i=1}^{N_{test}}(y_i-\hat{y}_i)^2}{\sum_{i=1}^{N_{test}}(y_i-\overline{y}_{train})^2} \quad (6)$$

2.4.2. RMSE

RMSE has the same units as the target (m/s) and penalises large errors more heavily than mean absolute error (MAE).

$$RMSE = \sqrt{\frac{1}{N_{test}}\sum_{i=1}^{N_{test}}(y_i - \hat{y}_i)^2} \quad (7)$$

2.4.3. Pearson correlation coefficient (r)

$\bar{y}_{test}$ and $\bar{\hat{y}}_{test}$ are the means of the observed and predicted values in the test set. The correlation coefficient provides a scale-independent measure of linear agreement.

$$r = \frac{\sum_{i=1}^{Ntest}(y_i - \bar{y}_{test})(\hat{y}_i - \bar{\hat{y}}_{test})}{\sqrt{\sum_{i=1}^{N_{test}}(y_i - \bar{y}_{test})^2}\sqrt{\sum_{i=1}^{N_{test}}(\hat{y}_i - \bar{\hat{y}}_{test})^2}} \quad (8)$$

2.5. Model selection criterion

To select the optimal feature subset, we applied a parsimony-based criterion. A candidate subset was considered satisfactory if it satisfied both conditions:

$$\begin{cases} RMSE_{test} \leq 1.05 \times RMSE_{best} \\ R^2_{test} \geq R^2_{best} - 0.02 \end{cases} \quad (9)$$

where $RMSE_{best}$ and R^2_{best} est are the best (lowest RMSE and highest R^2) values achieved across all eight subsets. Among all satisfactory subsets, the one with the smallest number of features was selected as the optimal model. This approach balances predictive accuracy with model simplicity, which is essential for integration into portable and wearable systems.

2.6. Feature importance quantification

Feature importance was computed using the out-of-bag (OOB) permutation method [20], which provides a model-agnostic, unbiased estimate of each feature's contribution. For each feature f, the importance score $\mathcal{I}(f)$ is defined as (10):

$$\mathcal{I}(f) = \frac{1}{B}\sum_{b=1}^{B}\left(err_{OOB}^{(b)} - err_{OOB,perm(f)}^{(b)}\right) \quad (10)$$

where:

- B is the number of trees.
- $err_{OOB}^{(b)}$ is the OOB prediction error of tree b (mean squared error for regression).
- $eerr_{OOB,perm(f)}^{(b)}$ is the OOB error after randomly permuting the values of feature f in the OOB samples.

A large positive importance score indicates that permuting the feature degrades prediction accuracy, implying that the feature is important. Scores are normalised to sum to 100% for interpretability.

2.7. Statistical analysis and reproducibility

All analyses were performed in MATLAB R2022b (The MathWorks, Inc.) using the statistics and machine learning Toolbox, with a fixed random seed (rng (42)) to ensure reproducibility. The relationship between age, blood pressure, and arterial stiffness is known to be non-linear and context-dependent [23], [24]. Our stratified sampling approach ensures that these relationships are adequately represented across the adult age spectrum.

3. RESULTS AND DISCUSSION

3.1. Feature importance analysis on the full feature set

Before presenting the ablation study results, we first analyse the relative contribution of each candidate variable using permutation-based feature importance scores derived from the full model (set 1, ten variables). This preliminary analysis serves as the foundation for the ablation study design: rather than defining feature subsets arbitrarily, each elimination step is guided by the importance ranking, ensuring a principled and interpretable reduction of the feature space. Figure 3 shows the normalised importance scores for all ten candidate features for both targets. Three tiers of importance are identifiable from Figures 3(a) and 3(b):

- Dominant tier: ba-PWV and fa-PWV jointly rank highest in Set 1 (15.8% and 13.5% for aPWV; 16.8% and 15.2% for cf-PWV), together with age. Both PWV indices encode the same underlying information, arterial wall stiffness, but split their importance across two correlated variables; replacing them with raw

ba-PTT (set 7) consolidates this into a single dominant predictor (63.9% for aPWV, 51.0% for cf-PWV). Age captures the complementary long-term dimension of cumulative arterial wall remodelling [1].

– Secondary tier: SBP and DBP contribute modestly but consistently for both targets, correcting the pressure-dependent component of stiffness, since higher transmural pressure transiently increases PWV independently of structural remodeling [5].
– Negligible tier: AIx, ABI, PPamp, MBP, and PP add little once the dominant and secondary predictors are available, being largely collinear with blood pressure and transit time [9].

This three-tier hierarchy directly motivates the four research questions addressed by the ablation study, and determines the order in which variables are removed across the eight subsets:

– Redundancy reduction: can the negligible-tier indices (AIx, ABI, PPamp) be removed without significant performance loss? (sets 1-2-3)
– Minimal haemodynamic set: what is the smallest set of blood pressure variables from the secondary tier that is required? (sets 3-4-5-6)
– Transit time representation: does the raw ba-PTT outperform the path-length-normalised ba-PWV? (set 6 vs. set 7)
– Age contribution: is age truly indispensable for accurate estimation? (set 7 vs. set 8)

The resulting eight feature subsets of decreasing size are summarised in Table 3.

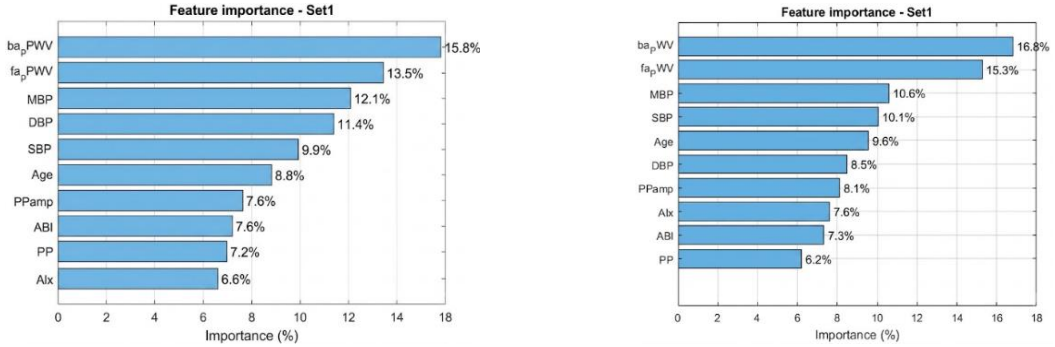


Figure 3. Normalised permutation-based feature importance for the full model (set 1): (a) aPWV target and (b) cf-PWV target. ba-PWV and fa-PWV rank highest because they are path-length-normalised surrogates of the pulse transit time; once ba-PTT replaces them (set 7), it consolidates their combined importance into a single dominant predictor

Table 3. Feature subsets evaluated in the ablation study. Targets: aPWV (invasive gold standard) and cf-PWV (non-invasive reference)

Subset	Features included	nf	Research question
Set 1	Age, ba-PWV, fa-PWV, AIx, ABI, PPamp, SBP, DBP, MBP, PP	10	Baseline (all variables)
Set 2	Age, ba-PWV, AIx, ABI, PPamp, SBP, DBP, MBP, PP	9	Q1 — remove fa-PWV
Set 3	Age, ba-PWV, PPamp, SBP, DBP, MBP, PP	7	Q1 — remove AIx, ABI
Set 4	Age, ba-PWV, SBP, DBP, MBP, PP	6	Q2 — remove PPamp
Set 5	Age, ba-PWV, SBP, DBP, MBP	5	Q2 — remove PP
Set 6	Age, ba-PWV, SBP, DBP	4	Q2 — remove MBP
Set 7	Age, ba-PTT, SBP, DBP	4	Q3 — raw transit time
Set 8	ba-PTT, SBP, DBP	3	Q4 — remove age

ba-PTT (raw, no path-length normalisation). Set 8 retains ba-PTT (not ba-PWV) to isolate the sole contribution of age while preserving the strongest individual predictor identified in Q3

3.2. Ablation study results for aPWV and cf-PWV target

The ablation study reveals a non-monotonic relationship between feature count and accuracy. Set 7 achieves the lowest RMSE (0.060 m/s) and highest R^2 (0.9984) using only four variables, outperforming the full ten-variable baseline (Set 1, RMSE = 0.096 m/s). Replacing ba-PWV with raw ba-PTT (set 6-set 7) reduces RMSE by 31%, while removing age (set 8) increases RMSE by 175%, confirming its critical role. Table 4 summarises the key subsets. The cf-PWV ablation follows the same pattern. Set 7 achieves RMSE = 0.113 m/s and R^2 = 0.9949, outperforming set 6 (RMSE = 0.122 m/s). Although set 1 reaches a marginally lower RMSE (0.099 m/s), it requires ba-PWV and fa-PWV, which are not obtainable without path-length measurement. Removing age (set 8) produces the largest degradation (+70% RMSE).

Table 4. Performance of the eight feature subsets for cf-PWV target. Bold: selected optimal model

Subset	Features	aPWV		cf-PWV	
		RMSE (m/s)	R^2	RMSE (m/s)	R^2
Set 1	All 10 variables	0.099	0.9960	0.096	0.9958
Set 2	Age, ba-PWV, AIx, ABI, PPamp, SBP, DBP, MBP, PP	0.148	0.9913	0.127	0.9926
Set 3	Age, ba-PWV, PPamp, SBP, DBP, MBP, PP	0.170	0.9883	0.150	0.9898
Set 4	Age, ba-PWV, SBP, DBP, MBP, PP	0.154	0.9903	0.127	0.9926
Set 5	Age, ba-PWV, SBP, DBP, MBP	0.132	0.9930	0.097	0.9956
Set 6	Age, ba-PWV, SBP, DBP	0.122	0.9940	0.087	0.9965
Set 7	Age, ba-PTT, SBP, DBP	0.113	0.9949	0.060	0.9984
Set 8	ba-PTT, SBP, DBP	0.192	0.9849	0.165	0.9875

Applying the parsimony criterion:

- For aPWV: only set 7 satisfies both conditions. Set 7 is the optimal model.
- For cf-PWV: both set 1 and set 7 satisfy conditions. Applying parsimony, set 7 is optimal, achieving equivalent accuracy with 60% fewer variables and no path-length measurement.

3.3. Comparison with the literature

Table 5 contextualises the proposed model against recent machine learning approaches to arterial stiffness estimation that report continuous regression metrics. Several observations emerge from this comparison. A clear distinction must be drawn between studies using simulated data and those using clinical cohorts: the near-perfect accuracy achieved here ($R^2 > 0.99$) reflects the noise-free, perfectly controlled ground truth of the simulated PWDB, and is not currently attainable in real-world clinical settings, as shown by the substantially lower performance of clinical studies (Chen *et al.* [13], $R^2 = 0.81$ on 1,944 subjects; Martinez-Rodrigo *et al.* [16], $R^2 = 0.79$ on 340 subjects). The reported metrics should therefore be read as an upper bound rather than a claim of clinical-grade accuracy. On the same simulated-data paradigm, Jin *et al.* [12] achieved $R^2 = 0.98$ (RMSE = 0.10 m/s) for cf-PWV using an RNN on RPW, comparable to the near-perfect accuracy obtained here ($R^2 = 0.9984$ for aPWV, $R^2 = 0.9949$ for cf-PWV). Regarding input modality, Jin *et al.* [12] rely on the RPW, which requires a tonometer or high-fidelity pressure sensor, while Chen *et al.* [13] and Martinez-Rodrigo *et al.* [16] use routine clinical markers that still require specialised equipment or multiple examinations. In contrast, the four variables used here, ba-PTT, age, SBP, and DBP, are all obtainable from a single dual-site cuff measurement, without any waveform acquisition or laboratory test, achieving comparable or better accuracy with fewer, more accessible inputs. A further distinctive feature of this work is the simultaneous evaluation of both the invasive (aPWV) and non-invasive (cf-PWV) reference standards on 1,200 age-stratified subjects (six groups, 200 each), whereas prior studies typically report only one target and do not stratify by age. Salvi *et al.* [3] showed that commercial cuff-based devices (BPLab, Mobil-O-Graph) estimate PWV almost entirely from age-squared and peripheral SBP, relying on indirect demographic surrogates with reproducibility that varies considerably across devices [25]. Our model shares a similar input space (age, SBP, DBP) but adds ba-PTT as a direct propagation measure, achieving near-perfect accuracy while eliminating the empirical distance estimation that limits current cuff-based algorithms, directly addressing the limitation identified by Salvi *et al.* [3] without additional hardware.

Table 5. Comparison with recent machine learning approaches for arterial stiffness estimation

Study	Method	Input	Target	Data	n	R^2	RMSE (m/s)
Jin *et al.* [12]	RNN	RPW	cf-PWV	simulated	4374	0.98	0.10
Zhang *et al.* [13]	Linear regression (LR), SVR, GB, RF, K-nearest neighbours (KNN)	baPWV, SBP, age	cf-PWV	Clinical	1944	0.81	N/A
Martinez-Rodrigo *et al.* [16]	RF, gradient boosting regression (GBR), SVR, NN	Clinical markers	aPWV	Clinical	340	0.79	0.98
Proposed (set 7)	RF	ba-PTT, age, SBP, DBP	aPWV	simulated	1200	0.9984	0.060
Proposed (set 7)	RF	ba-PTT, age, SBP, DBP	cf-PWV	simulated	1200	0.9949	0.113

4. CONCLUSION

This study demonstrates that accurate estimation of both invasive aPWV and non-invasive cf-PWV is achievable from four clinically accessible variables: ba-PTT, age, systolic blood pressure, and diastolic blood pressure, all obtainable from a standard dual-site cuff measurement without specialised sensors or

waveform acquisition. Feature importance analysis and systematic ablation across eight nested subsets identified this four-variable model (set 7) as optimal under a parsimony criterion. Three findings stand out: raw transit time substantially outperforms derived ba-PWV (31% lower RMSE for aPWV); age is indispensable, its removal increasing RMSE by 175%; and the model achieves state-of-the-art accuracy on simulated data (R^2 = 0.9984 for aPWV, R^2 = 0.9949 for cf-PWV), well above clinical benchmarks (R^2 = 0.79-0.81) while using fewer inputs than most comparable approaches.

This approach does not replace invasive or cf-PWV measurement, but offers a practical alternative for routine monitoring in ambulatory, home-based, or low-resource settings. Its main limitation is reliance on the simulated PWDB, which provides noise-free ground truth but does not capture real-world confounders such as comorbidities, medication, or sensor noise; reported performance should be read as an upper bound. Future work will focus on external clinical validation, domain adaptation to bridge the simulation-to-reality gap, and integration into portable, wearable monitoring systems.

ACKNOWLEDGMENTS

The authors would like to thank the research team of the LIST Laboratory (University of Boumerdes, Algeria), Cardiology department (Hospital of Mons, Belgium) and University of Mons (Belgium) for their valuable support during this work.

FUNDING INFORMATION

Dr Stéphane Carlier was supported for this work by the VASCULAI project, supported by the European Union through the Interreg France–Wallonie–Vlaanderen (FWVL) program (ref. 0100224). Dr Omari Tahar received a travel grant of the Fonds de mobilité WBI–Maghreb Liban 2025 - S2 (visa n SUB/2025/676790).

AUTHOR CONTRIBUTIONS STATEMENT

This journal uses the Contributor Roles Taxonomy (CRediT) to recognize individual author contributions, reduce authorship disputes, and facilitate collaboration.

Name of Author	C	M	So	Va	Fo	I	R	D	O	E	Vi	Su	P	Fu
Lilia Radjef	✓	✓	✓	✓	✓	✓								
Tahar Omari	✓	✓		✓	✓	✓	✓	✓	✓	✓	✓	✓		✓
Karim Baiche		✓		✓						✓	✓	✓	✓	
Stéphane Carlier		✓		✓						✓	✓	✓	✓	✓

C : **C**onceptualization
M : **M**ethodology
So : **So**ftware
Va : **Va**lidation
Fo : **Fo**rmal analysis
I : **I**nvestigation
R : **R**esources
D : **D**ata Curation
O : Writing - **O**riginal Draft
E : Writing - Review & **E**diting
Vi : **Vi**sualization
Su : **Su**pervision
P : **P**roject administration
Fu : **Fu**nding acquisition

CONFLICT OF INTEREST STATEMENT

The authors declare no conflicts of interest.

DATA AVAILABILITY

The PWDB is publicly available at https://peterhcharlton.github.io/pwdb/.

REFERENCES

[1] C. Vlachopoulos, K. Aznaouridis, and C. Stefanadis, "Prediction of Cardiovascular Events and All-Cause Mortality With Arterial Stiffness," *Journal of the American College of Cardiology*, vol. 55, no. 13, pp. 1318–1327, Mar. 2010, doi: 10.1016/j.jacc.2009.10.061.

[2] G. F. Mitchell *et al.*, "Arterial stiffness and cardiovascular events: the Framingham Heart Study," *Circulation*, vol. 121, no. 4, pp. 505–511, 2010. doi: 10.1161/CIRCULATIONAHA.109.886655.

[3] P. Salvi *et al.*, "Noninvasive estimation of aortic stiffness through different approaches: comparison with intra-aortic recordings," *Hypertension*, vol. 74, no. 1, pp. 117–124, 2019. doi: 10.1161/HYPERTENSIONAHA.119.12853.

[4] M. F. O'Rourke and J. Hashimoto, "Mechanical Factors in Arterial Aging," *Journal of the American College of Cardiology*, vol.

50, no. 1, pp. 1–13, Jul. 2007, doi: 10.1016/j.jacc.2006.12.050.
[5] S. Laurent *et al*., "Expert consensus document on arterial stiffness: methodological issues and clinical applications," *European Heart Journal*, vol. 27, no. 21, pp. 2588–2605, Sep. 2006, doi: 10.1093/eurheartj/ehl254.
[6] Y. Ben-Shlomo *et al.*, "Aortic Pulse Wave Velocity Improves Cardiovascular Event Prediction," *Journal of the American College of Cardiology*, vol. 63, no. 7, pp. 636–646, Feb. 2014, doi: 10.1016/j.jacc.2013.09.063.
[7] H. Tanaka and M. Safar, "Influence of lifestyle modification on arterial stiffness and wave reflections," *American Journal of Hypertension*, vol. 18, no. 1, pp. 137–144, Jan. 2005, doi: 10.1016/j.amjhyper.2004.07.008.
[8] T. Ohkuma *et al.*, "Brachial-Ankle Pulse Wave Velocity and the Risk Prediction of Cardiovascular Disease," *Hypertension*, vol. 69, no. 6, pp. 1045–1052, Jun. 2017, doi: 10.1161/hypertensionaha.117.09097.
[9] L. M. V. Bortel *et al*., "Expert consensus document on the measurement of aortic stiffness in daily practice using carotid-femoral pulse wave velocity," *Journal of Hypertension*, vol. 30, no. 3, pp. 445–448, Mar. 2012, doi: 10.1097/hjh.0b013e32834fa8b0.
[10] J. Alastruey, K. H. Parker, and S. J. Sherwin, "Arterial pulse wave haemodynamics," in *Proc. 11th International Conference on Pressure Surges*, pp. 401-443, 2012.
[11] J. Li, K. Zhu, and L. Pan, "Wrist and finger motion recognition via M-mode ultrasound signal: A feasibility study," *Biomedical Signal Processing and Control*, vol. 71, p. 103112, Jan. 2022, doi: 10.1016/j.bspc.2021.103112.
[12] W. Jin, P. Chowienczyk, and J. Alastruey, "Estimating pulse wave velocity from the radial pressure wave using machine learning algorithms," *PLoS ONE*, vol. 16, no. 6, p. e0245026, 2021. doi: 10.1371/journal.pone.0245026.
[13] M. Chen, J. Xiong, M. Li, T. Hu, and Y. Zhang, "Research on Prediction model of Carotid-Femoral Pulse Wave Velocity: Based on Machine Learning Algorithm," *The Journal of Clinical Hypertension*, vol. 27, no. 3, Mar. 2025, doi: 10.1111/jch.70017.
[14] K. P. Abrisham, K. Alipour, B. Tarvirdizadeh, and M. Ghamari, "Advancing PPG-based cf-PWV estimation with an integrated CNN-BiLSTM-Attention model," *Signal, Image and Video Processing*, vol. 18, no. 12, pp. 8621–8633, Aug. 2024, doi: 10.1007/s11760-024-03496-4.
[15] G. Tse *et al*., "Relationship between angiotensin-converting enzyme inhibitors or angiotensin receptor blockers and COVID-19 incidence or severe disease," *Journal of Hypertension*, vol. 39, no. 8, pp. 1717–1724, Apr. 2021, doi: 10.1097/hjh.0000000000002866.
[16] A. Martinez-Rodrigo, J. Pedrosa, D. Carneiro, I. Cavero-Redondo, and A. Saz-Lara, "Development of a Non-Invasive Clinical Machine Learning System for Arterial Pulse Wave Velocity Estimation," *Applied Sciences*, vol. 15, no. 9, p. 4788, Apr. 2025, doi: 10.3390/app15094788.
[17] Z. Zhou *et al.*, "Development of an interpretable machine learning model for early prediction of aortic stiffness risk in health examination populations," *Frontiers in Cardiovascular Medicine*, vol. 12, Jan. 2026, doi: 10.3389/fcvm.2025.1730409.
[18] H. Hellqvist, M. Karlsson, J. Hoffman, T. Kahan, and J. Spaak, "Estimation of aortic stiffness by finger photoplethysmography using enhanced pulse wave analysis and machine learning," *Frontiers in Cardiovascular Medicine*, vol. 11, Mar. 2024, doi: 10.3389/fcvm.2024.1350726.
[19] J. M. Vargas, M. A. Bahloul, and T.-M. Laleg-Kirati, "A learning-based image processing approach for pulse wave velocity estimation using spectrogram from peripheral pulse wave signals: an in silico study," *Frontiers in Physiology*, vol. 14, Mar. 2023, doi: 10.3389/fphys.2023.1100570.
[20] P. H. Charlton, J. M. Harana, S. Vennin, Y. Li, P. Chowienczyk, and J. Alastruey, "Pulse Wave Database (PWDB): Baseline subjects aged 25 to 75." *Zenodo*, Jul. 17, 2019. doi: 10.5281/ZENODO.3339559.
[21] L. Breiman, "Random Forests," *Machine Learning*, vol. 45, no. 1, pp. 5–32, Oct. 2001, doi: 10.1023/a:1010933404324.
[22] A. Ayadi, I. Hammami, W. Sahtout, and O. Baledant, "Improving arterial stiffness prediction with machine learning utilizing hemodynamics and biomechanical features derived from phase contrast magnetic resonance imaging," *Proceedings of the Institution of Mechanical Engineers, Part H: Journal of Engineering in Medicine*, vol. 238, no. 11–12, pp. 1120–1132, Nov. 2024, doi: 10.1177/09544119241291191.
[23] C. M. McEniery, I. B. Wilkinson, and A. P. Avolio, "Age, hypertension and arterial function," *Clinical and Experimental Pharmacology and Physiology*, vol. 34, no. 7, pp. 665–671, 2007. doi: 10.1111/j.1440-1681.2007.04657.x.
[24] "Determinants of pulse wave velocity in healthy people and in the presence of cardiovascular risk factors: 'establishing normal and reference values,'" *European Heart Journal*, vol. 31, no. 19, pp. 2338–2350, Jun. 2010, doi: 10.1093/eurheartj/ehq165.
[25] T. Papaioannou, A. Protogerou, K. Stamatelopoulos, M. Vavuranakis, and C. Stefanadis, "Non-Invasive Methods and Techniques for Central Blood Pressure Estimation: Procedures, Validation, Reproducibility and Limitations," *Current Pharmaceutical Design*, vol. 15, no. 3, pp. 245–253, Jan. 2009, doi: 10.2174/138161209787354203.

BIOGRAPHIES OF AUTHORS



Lilia Radjef received her Master's degree in Biomedical Engineering in 2021. In March 2022, she was admitted to the national Doctoral programme in Biomedical Engineering at M'Hamed Bougara University of Boumerdes, Algeria. She is a member of Laboratory Engineering Systems and Telecommunications (LIST) at the Faculty of Technology. Her doctoral research focuses on arterial stiffness assessment and biomedical signal processing. She can be contacted at email: l.radjef@univ-boumerdes.dz.



Tahar Omari received the Engineer degree in Biomedical Engineering in 2006, the M.Sc. degree in 2009, and the Ph.D. degree in 2017 from the University of Tlemcen, Algeria, followed by the Habilitation (HDR) in 2019 from the same institution. He is currently an Associate Professor at the University of Ain Temouchent, Algeria, where he teaches programming and biomedical instrumentation. His research covers cardiovascular monitoring, non-invasive blood pressure estimation, pulse transit time analysis, and arterial stiffness assessment. He can be contacted at email: tahar.omari@univ-temouchent.edu.dz.



Karim Baiche received the Engineer degree in Electronics, Control Engineering in 1992 from the university of Setif, Algeria, The M.Sc. (Magister) degree in Applied Automation from the Institute of Hydrocarbons and Chemistry (INHC)-Boumerdes in 1998 and received his Ph.D. from the University of MHamed Bougara Boumerdes, Algeria in 2014. He obtained the Habilitation (HDR) in Electrical Engineering, Control Engineering and Signal processing from the same university in 2019. He is currently a full Professor at the University of M'Hamed Bougara Boumerdes, Algeria, where he is involved in teaching and practical training in telecommunications and biomedical instrumentation. He can be contacted at email: kbaiche@univ-boumerdes.dz.



Stéphane Carlier received the M.D. degree in Cardiology in 1996 from the Université Libre de Bruxelles (ULB), Belgium, and the Ph.D. degree in Bioengineering in 2001 from Erasmus University Rotterdam, the Netherlands. He is currently a cardiologist and head of the cardiology department at CHU Helora (site Kennedy) in Mons, Belgium, and a Professor of Cardiology at the University of Mons (UMONS), where he teaches cardiovascular medicine and intravascular imaging. His research covers intravascular imaging (IVUS, OCT), plaque rupture modeling, noninvasive cardiovascular monitoring, pulse transit time analysis, and arterial stiffness assessment. He can be contacted at email: stephane.carlier@umons.ac.be.